

Electronic Supplementary Information (ESI)

Kinetically Modulated Specificity against Single-base Mutants in Nucleic Acid Recycling Circuitry Using Destabilization Motif

Tsz Wing Fan[†] and I-Ming Hsing^{†‡*}

[†]Department of Chemical and Biomolecular Engineering and [‡]Division of Biomedical Engineering, The Hong Kong
University of Science and Technology, Hong Kong

*Email: kehising@ust.hk

S1. Specificity of HCR and Target Recycling based Amplification (TRBA) against time

This section demonstrates the difference between Hybridization Chain Reaction (HCR), a typical example where the signal amplification process is decoupled from analyte recognition, and target recycling assisted amplification in sustaining detection specificity against time. For simplicity, in both derivations we assume much excess probes or hairpins concentrations in the system such that they can be treated as a constant.

S1.1 Hybridization Chain Reaction (HCR)

In HCR, signal amplification mainly relies on the autonomous assembly of the two metastable hairpins (H1 and H2), but this process is initiated only when one of these hairpins is successfully opened up by the analyte. Assume in the system we have highly excess hairpins and the time required by a single T or SBM to open up one H1 is t and $\beta \cdot t$ respectively, where β is a modifying factor to indicate the longer time needed by the SBM to trigger the reaction as compared to T (i.e. $\beta > 1$); while it takes the same time r for the subsequent and alternate hybridization of each H1 and H2 onto the growing polymer chain (Fig. S1).

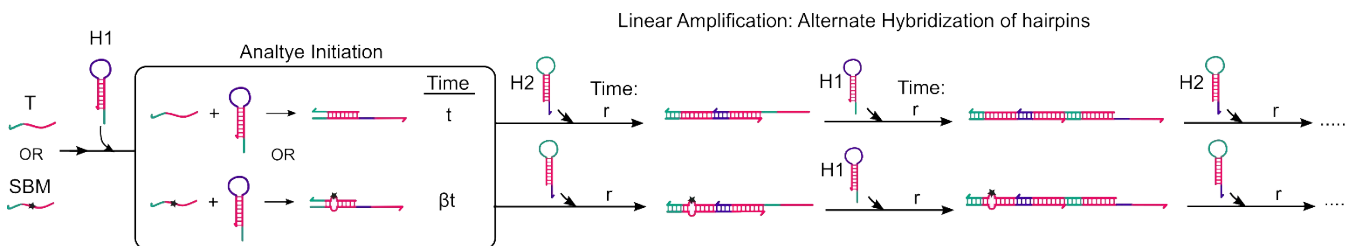


Fig. S1. Schematics of the first few steps of Hybridization Chain Reaction (HCR), where H1 and H2 are two hairpins for linear signal amplification upon one of them is triggered by the analyte, either Target (T) or the Single Base Mutant (SBM). t and βt are the time required for T and SBM to successfully open up H1, while r is the time needed for subsequent assembly of each H1 or H2 onto the growing polymer chain.

If signal is given whenever H1 or H2 is unwound, time required for T and SBM to give the first signal is t and βt respectively, which corresponds to their time in activating H1; $t + r$ and $\beta t + r$ to produce two signals, where both require additional time r for interacting with H2; $t + 2r$ and $\beta t + 2r$ to produce three signals, with extra time r added for interacting with H1; similarly $t + 3r$ and $\beta t + 3r$ for generating four signals; and so on. In such, to produce n signals, total time required by T and SBM is thus $t + (n - 1)r$ and $\beta t + (n - 1)r$ respectively (Fig. S2).

Hybridization Chain Reaction (HCR)

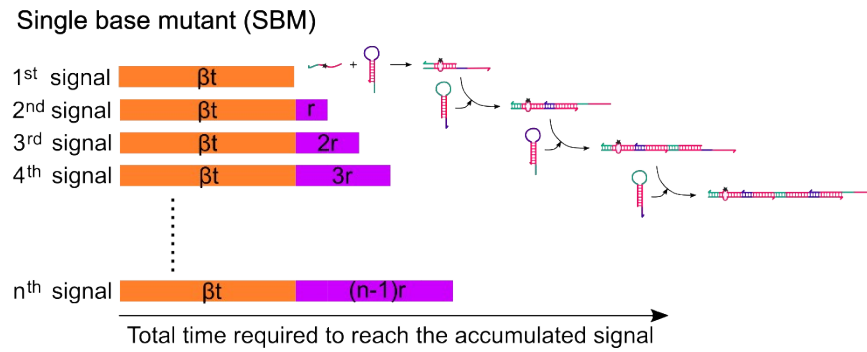
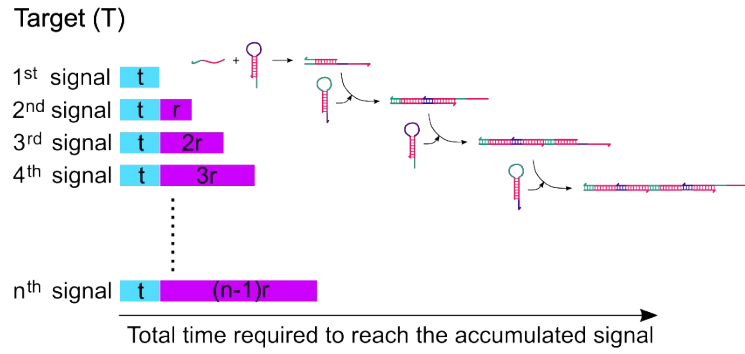


Fig. S2 Time requirement for T and SBM to reach the signal in HCR.

Let n_T and n_{SBM} be the total number of signals achieved by T and SBM respectively when the time of detection equals to D . For example,

$$t + (n_T - 1)r = D \quad (1)$$

$$\beta t + (n_{SBM} - 1)r = D \quad (2)$$

By simple algebraic calculation, we could get

$$n_T = \frac{D - t + r}{r} \quad (3)$$

$$n_{SBM} = \frac{D - \beta t + r}{r} \quad (4)$$

Therefore, discrimination factor (DF) can be obtained by dividing equation (3) by (4)

$$DF = \frac{n_T}{n_{SBM}} = \frac{D - t + r}{D - \beta t + r} \quad (5)$$

Here, we could notice that DF is dependent and is a function of the detection time D. As time scale for $D \gg t$ or r , and the analyte recognition is usually the rate limiting step of the reaction where subsequent hybridization of hairpins is relatively faster, i.e. $t \gg r$ or $r \sim 0$, equation (3) can be simplified as

$$DF = \frac{1 - \left(\frac{t}{D}\right)}{1 - \beta\left(\frac{t}{D}\right)} \quad (6)$$

From the result, it is notable that only if β , the time multiplying factor of SBM is in particular order of magnitude to t/D , will it give significant specificity against spurious SBM.

In typical toehold strand displacement reaction, analyte initiation can be described by



Where SP and P are sensing probe and product respectively.

Assume SP (or H1 in HCR) is in excess,

$$\frac{d[P]}{dt} = k_{f,T}[SP]_0([T]_0 - [P]) \quad (8)$$

$$\frac{d[P]}{dt} = k_{f,SBM}[SP]_0([SBM]_0 - [P]) \quad (9)$$

Where $[SP]_0$ and $[T]_0$ are the initial concentrations of SP and T.

Through kinetic derivation, we get time required to reach certain signal $[P]$ for T and SBM is respectively

$$t_T = \frac{1}{k_{f,T}[SP]_0} \ln \frac{[T]_0}{[T]_0 - [P]} \quad (10)$$

$$t_{SBM} = \frac{1}{k_{f,SBM}[SP]_0} \ln \frac{[SBM]_0}{[SBM]_0 - [P]} \quad (11)$$

Therefore, at equimolar concentrations of $[T]$ and $[SBM]$ (i.e. $[T]_0 = [SBM]_0$),

$$\beta = \frac{t_{SBM}}{t_T} = \frac{k_{f,T}}{k_{f,SBM}} \quad (12)$$

From literature, $k_{f,T}$ for SP with a toehold length of 7 nt will be around $1.2 \times 10^6 M^{-1} s^{-1}$; while $k_{f,SBM}$ depends on both the position and identity of mismatch and on average $\frac{k_{f,T}}{k_{f,SBM}} = 5$. Using this value of β and put it back to equation (6), a plot of DF against t/D from 10^{-10} to 10^{-1} is given (Fig. S3).

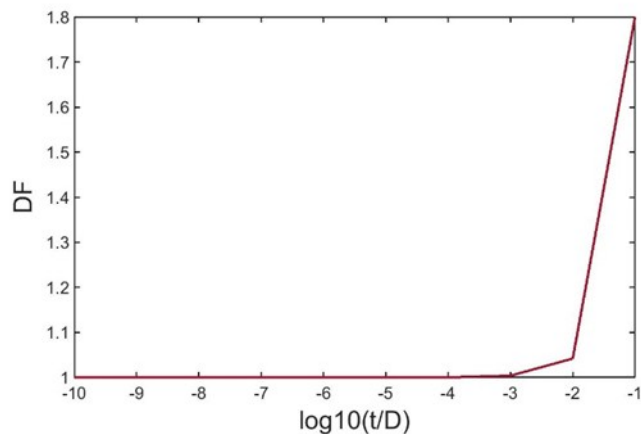


Fig. S3 A plot of DF against logarithm of t/D , where $DF = \frac{1 - \left(\frac{t}{D}\right)}{1 - k\left(\frac{t}{D}\right)}$ and $\beta = 5$.

Along the detection where D is increasing, t/D will become smaller and closer to 0 and eventually $DF \sim 1$.

S1.2 Target Recycling based Amplification Approach (TRBA)

Unlike HCR, TRBA requires interaction between probe and analyte at every cycle, providing sustainable detection specificity against time. To show this, we conduct an analytical derivation similar to the case of HCR. Like HCR, we assume the time required for every single T and SBM to interact with the Probe is t and βt respectively. Again, β is the multiplying factor indicating the longer time for SBM involved in the interaction. They would produce one signal for every successful interaction with the Probe (indicated by the yellow pentagon in Fig. S4). For the T and SBM to react with another probe, they have to be recycled, for example, being displaced from the probe and analyte complex by an assistant strand. To

have a fair comparison with the HCR process, we assume the time taken for this recycling process is identical for both T and SBM and equals to r .

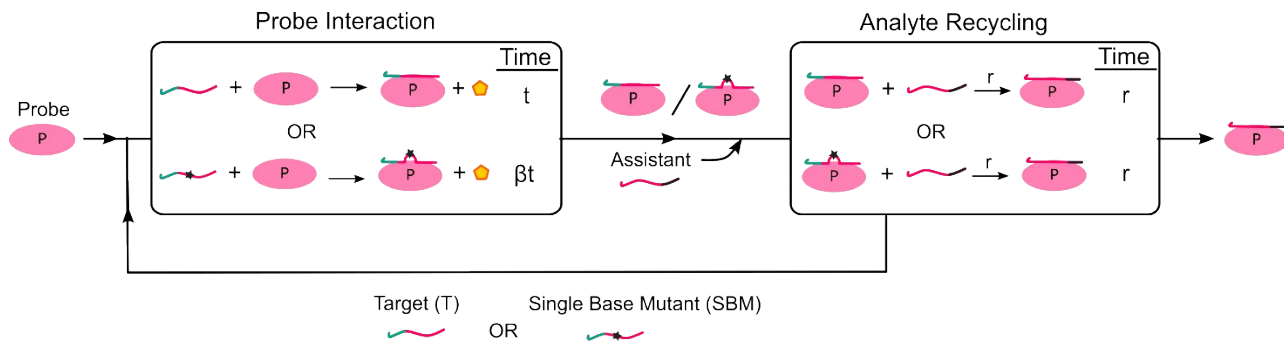


Fig. S4. Schematics of TRBA, where T and SBM interact with the Probe by time t and βt respectively; and they are recycled with time r . The yellow pentagon represents the signal given once the probe successfully reacts with the analyte.

So, the first signal will be given out at time t and βt for T and SBM respectively when they successfully interact with the probe. Then, a second signal will be given after they are recycled and interact with another probe, which equals to $2t + r$ and $2\beta t + r$ correspondingly; $3t + 2r$ and $3\beta t + 2r$ for the third signal; $4t + 3r$ and $4\beta t + 3r$ for the forth; and following this deduction, T and SBM would require $nt + (n - 1)r$ and $n\beta t + (n - 1)r$ respectively to achieve a total of n signals (Fig. S5).

Target Recycling based Amplification (TRBA)

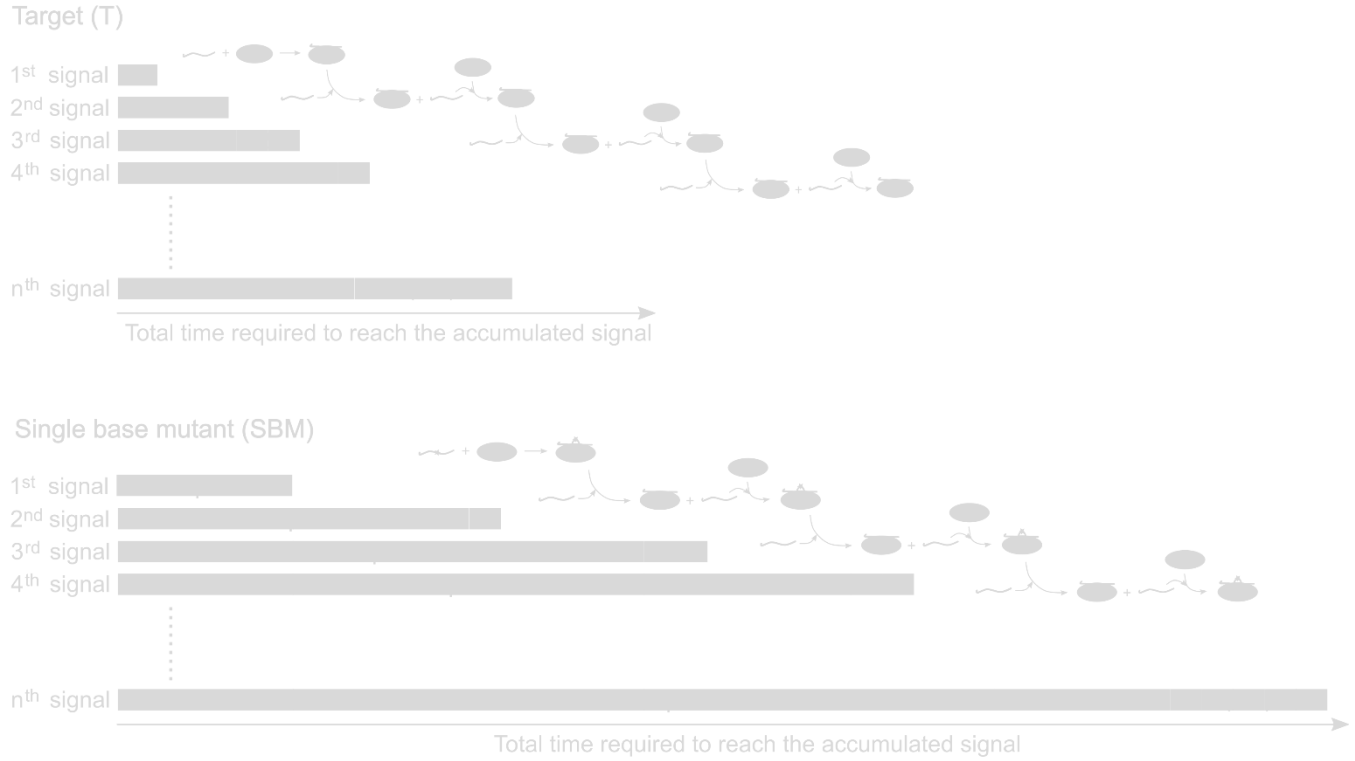


Fig. S5. Time requirement for the specified signal production in TRBA. The width of the bar represents the relative quantity of the time constants.

When the detection time equals to D , the number of signals achieved by T and SBM is thereby

$$n_T = \frac{D + r}{t + r} \quad (13)$$

$$n_{SBM} = \frac{D + r}{\beta t + r} \quad (14)$$

Therefore,

$$DF = \frac{n_T}{n_{SBM}} = \frac{\beta t + r}{t + r} \quad (15)$$

We could see now DF is independent of the detection time D and is simply a constant function. This implies that the discrimination factor can be sustained even for long period of measurement in opposite

to that of HCR. Also, like HCR, if we assume the analyte recognition is the rate limiting step and the recycling process occurs relatively much faster (i.e. $r \ll t$ or $r \sim 0$), DF simply equals to β or $\frac{k_{f,T}}{k_{f,SBM}}$.

But if the time for probe interaction is comparable to analyte recycling (i.e. $r \sim t$), equation (15) would then become

$$DF = \frac{t(\beta + 1)}{2t} = \frac{\beta + 1}{2} \quad (16)$$

As $\beta > 1$, DF will be trimmed in this case.

In another extreme case, if recycling becomes the rate limiting step (i.e. $r \gg t$),

$$DF = \frac{\beta t + r}{r} = \beta \left(\frac{t}{r}\right) + 1 \quad (17)$$

Consider if $DF \geq \beta$

$$\beta \left(\frac{t}{r}\right) + 1 \geq \beta \quad (18)$$

$$\beta \leq \frac{1}{1 - \frac{t}{r}} \quad (19)$$

As $r \gg t$ and $\frac{t}{r} \sim 0$, equation (19) becomes

$$\beta \leq 1 \quad (20)$$

However, this contradicts with the assumption that $\beta > 1$ which implies we could not achieve equal or even larger discrimination factor than β in this condition. This therefore shows that if the recycling step is either comparable to probe interaction or becomes the rate limiting step of the overall reaction, the specificity would be lessened compared to the single reaction of probe hybridization. Therefore, to sustain and maximize the specificity, the probe interaction should be designed as the rate limiting step of the system while having a fast analyte recycling step.

S2. Energy level diagram explaining the specificity enhancement by shorter A1

From the deduction in Section S1, it is noted that specificity of TRBA is sustained with time by the discrimination factor β , which is the multiplying factor of time by which the mismatched target needs to reach the same signal as that of the correct counterpart. In this sense, increasing β helps to increase the

overall detection specificity. Fig. S6 shows the energy diagrams of the entire reactions that depict how our system could increase β and achieve the specificity enhancement kinetically using shorter and longer assistants A1.

In our system, reactions can be broken down into three elementary steps: 1) the interaction of the Sensing Probe (SP) and analyte (i.e. T or SBM) to partially open the sequestered domains of SP; 2) the removal of Q strand from SP by A1; and 3) analyte recycling by the toehold exchange reaction of A2 on I3. In these reactions, we specially designed the first reaction to be rate limiting, for example, highest forward activation energy for the first step of reaction $Ea_{1,f}$ than the latter two ($Ea_{2,f}$ and $Ea_{3,f}$). This is achieved by setting the toehold length of SP the shortest (i.e. 5nt overhang on SP) among other sequestered toeholds (i.e. 6nt for the toeholds that A1 would anchor; and 10nt for toeholds that A2 associates). This is such to make the overall rate of reactions highly dependent of the analyte recognition by SP, or the value of β .

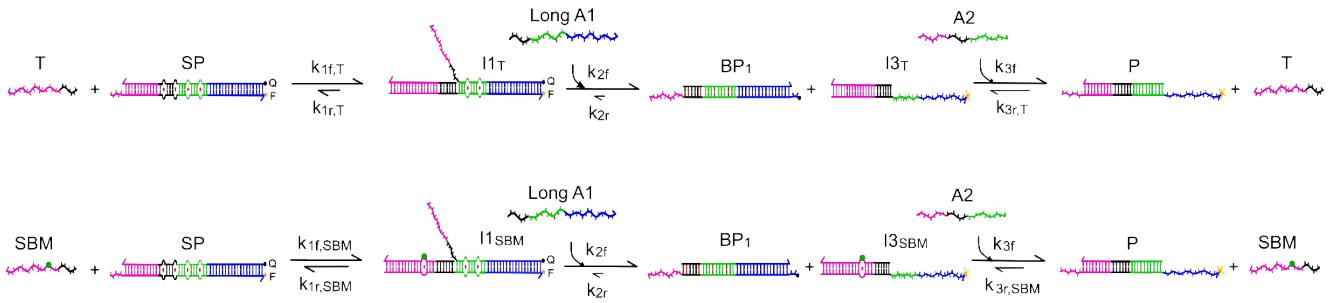
As forward rate of the reaction mainly depends on toehold association or the length of toeholds, we assume that $Ea_{1,f}$, $Ea_{2,f}$ and $Ea_{3,f}$ (or $k_{1,f}$, $k_{2,f}$ and $k_{3,f}$) are identical for the reactions with T or SBM, and with long or short A1 because toehold lengths of the reactants in these reactions remain the same. However, the backward activation energy for the first reaction $Ea_{1,b}$ (or $k_{1,r}$) varies among the four cases studied (i.e. $k_{1,r,T} < k_{1,r,SBM}$ and values differ while using long and short A1).

When long A1, for example, strand with the black domain is used, T or SBM just needs to partially displace the Q strand of SP up to the black domain, which would then act as a toehold for long A1 to associate. The net enthalpy gain in this strand displacement process renders both T and SBM to perform the forward reaction (i.e. $Ea_{1,b} > Ea_{1,f}$ and $k_{1,f} > k_{1,r}$), even though SBM reacts less favorably and slower than T (i.e. $Ea_{1,b} \text{ of } T > Ea_{1,b} \text{ of } SBM$ and $k_{1,r,SBM} > k_{1,r,T}$) as accounted by the difference in Gibbs free energies of the intermediate 1 formed (i.e. $\Delta G = I1_{SBM} - I1_T$). Also, as $Ea_{2,f} > Ea_{1,b}$ of both T and SBM, it means that once $I1_{SBM}$ or $I1_T$ is formed, they tend to react forwardly with long A1 to form BP_1 and $I3_T$ (or $I3_{SBM}$), rather than reforming SP. The high enthalpy drive of these reactions limits the differentiation between T and SBM.

In contrast, when short A1, for example, strand without the black domain is used, Q strand of SP has to be opened up to the green domain for short A1 to anchor. Since T and SBM only reacts with SP and displaces Q strand up to the black domain, few base pairs of the green domains of SP have to be spontaneously dissociated. This in fact mimics a toehold exchange reaction in which the enthalpy gain in

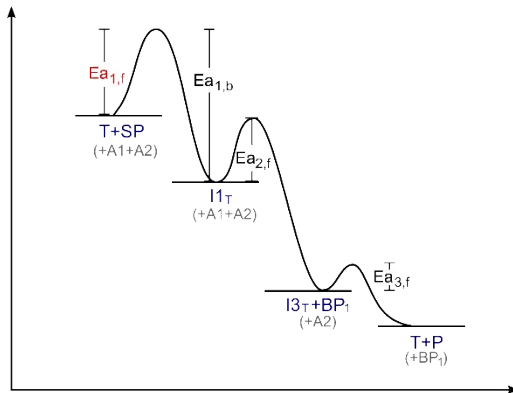
base pairing of the exposed toehold balances the enthalpy loss in the spontaneous dissociation of the sequestered green domain. So now, the reaction Gibbs free energy for the interaction between SP and T is just slightly less than 0, which means the reaction is still slightly tending forward (i.e. $Ea_{1,f} < Ea_{1,b}$ or $k_{1f,T} > k_{1r,T}$). As $I2_T$ formed is preferentially consumed by the short A1 than reforming SP ($Ea_{2,f} < Ea_{1,b}$), this further facilitates the reaction forward despite slower reaction than using long A1. However, in the case of SBM which reacts with SP to form $I2_{SBM}$, the reaction becomes non-spontaneous and tending backward (i.e. $Ea_{1,b} < Ea_{1,f}$ or $k_{1f,SBM} < k_{1r,SBM}$). Also, this decrease in the backward activation energy in the reaction between probe and SBM also decreases the spontaneity of subsequent removal of Q strand by A1, for example, $Ea_{1,b} < Ea_{2,f}$. This shows that even when $I2_{SBM}$ is formed, it is more likely to reform SP than to react with short A1 for ongoing reactions. In other words, subsequent reactions happen only when a pre-equilibrium between SBM and SP is reached. The non-spontaneity of these reactions thereby produces negligible signals and confers high specificity against spurious targets using short A1.

Long A1:



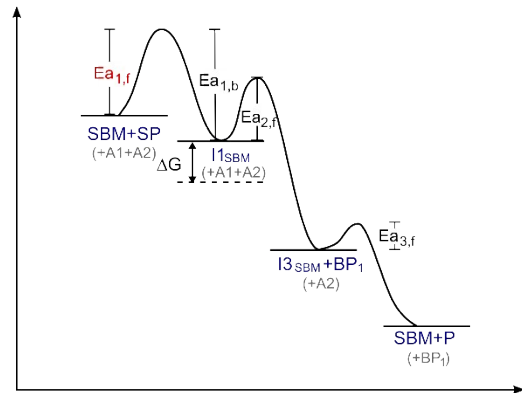
Target

Energy Level

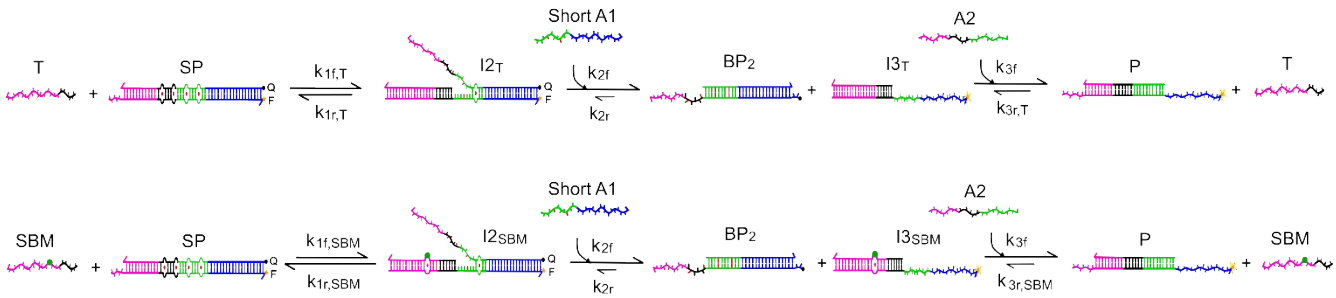


Single Base Mutant

Energy Level

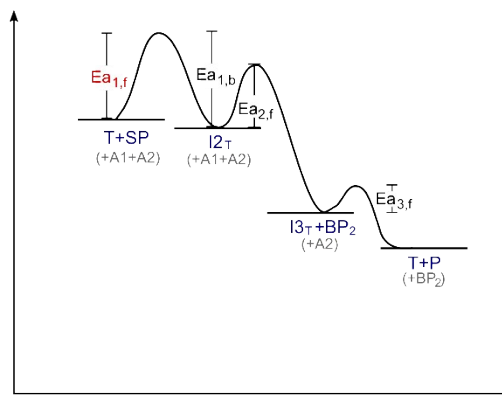


Short A1:



Target

Energy Level



Single Base Mutant

Energy Level

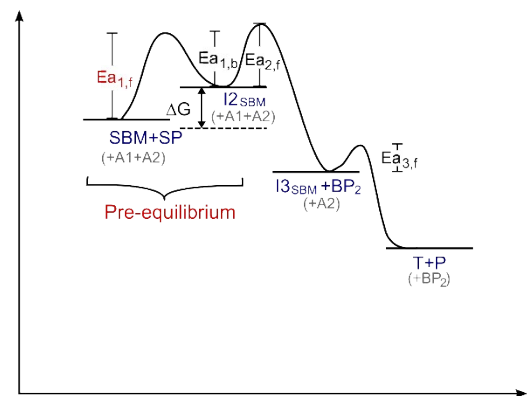


Fig. S6 Free energy level diagrams of the system using long and short A1 against T or SBM. E_a refers to activation energy; number in the subscript corresponds to the elementary steps of the reactions (1: reaction between probe and analyte; 2: reaction between A1 and I1 (or I2); and 3: reaction between A2 and I3) while f and b refers to forward and backward. Components shown under the energy states are highlighted in blue to refer the reactants or products involved in the reactions making the change in energy levels, while in grey to represent uninvolved reactants and products at the particular stage.

S3. Detailed Component Design and Reaction Mechanism

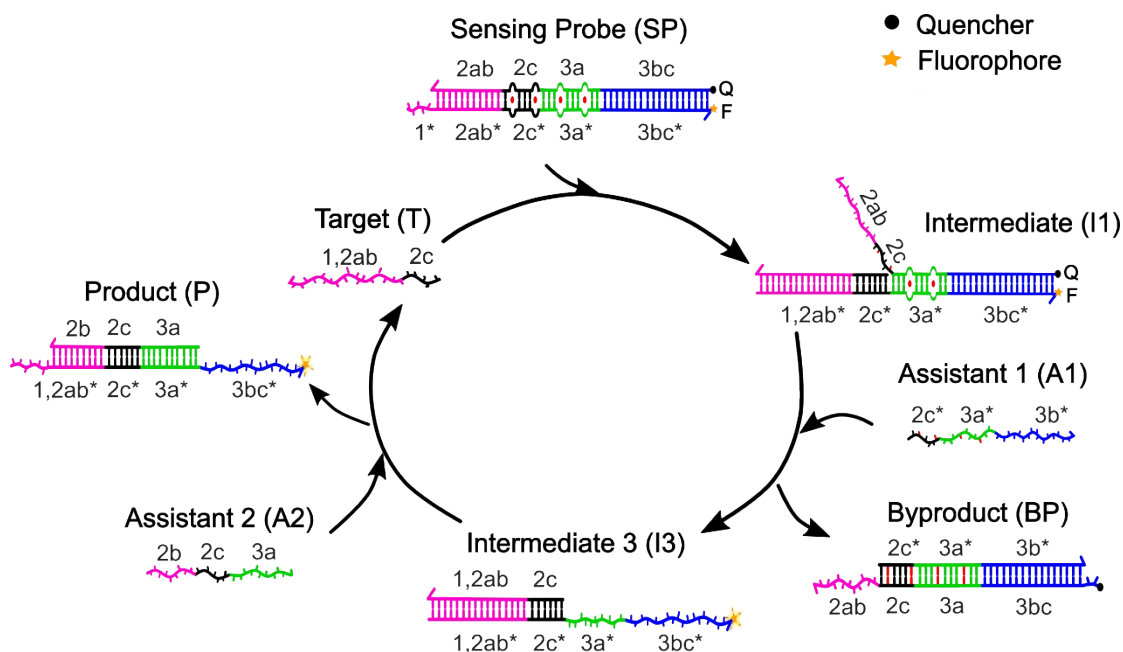


Fig. S7 Detailed mechanism of the system using long A1. Strands are labelled with color, numbers and alphabet; where domains with same number and alphabet indicate the same sequence; and * thereon indicate complementarity to those without (i.e. 2b and 2b*); Short strips on the strand represent each single base, while colored in red to indicate base mutation, which hybridizes only to their complementary strip labeled in red, otherwise forming mismatch bubbles (the red dots).

S4. Sensing Probe Characterization

The design of Sensing Probe, such as the quantity and position of mutated bases (i.e. mismatches/insertions) introduced, as well as its length, closely relates to system stability and reaction kinetics. For example, too many bases mutated in the destabilization motif lower stability of SP and therefore increase the chance for other system components to invade even in the absence of target; whereas too few bases form a highly thermostable SP which hinders spontaneous dissociation and reduces its kinetics and

spontaneity in interacting with shorten A1. Therefore, a detailed characterization on the design of Sensing Probe was conducted through PAGE experiments to analyze their recycling performance and leakage issue like the one shown in main text (Fig. 2A).

S4.1 Effect of Destabilization Motif. Destabilization motif on the Sensing Probe (SP) serves three main functions: 1) lower local thermodynamics to facilitate spontaneous dissociation; 2) increase reaction spontaneity by additional enthalpy gained between complementary A1 and Q strand; and 3) reduce crosstalk between A1 and A2, which inherit 16bp complementarity in sequence (see Fig. 1 in main Text). The last function, confines the design of destabilization motif by not placing the mutations too far from each other. Knowing that at least 4bp is necessary to form stable duplex,¹ intermittent mismatches or insertions were introduced to the particular region forming eight sets of destabilization motifs (Fig. S8). To ensure fair comparison, sequence of set 1-6 and set 7-8 were kept exactly the same except the destabilization motifs. The blue domain was designed to be 18bp long enough for stabilization such that any variation in reaction performance is owing to the change of destabilization motif.

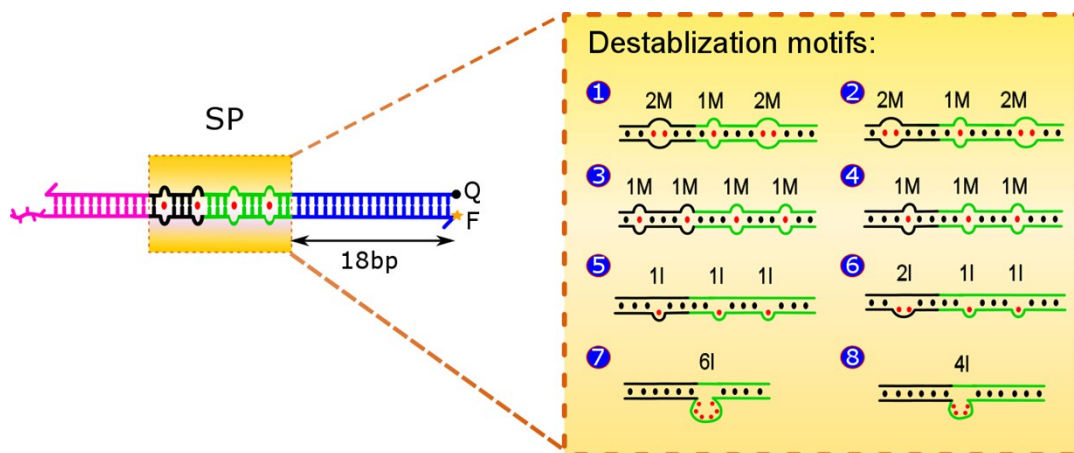


Fig. S8 Eight sets of destabilization motif were designed and introduced to the 16bp complementary region of SP either by insertions or mismatches. Each dot represents a base/ base pair; M and I correspond to mismatch and insertion respectively. To ensure a fair comparison among motifs, sequence of set 1-6 and set 7-8 were kept exactly the same except the destabilization motif domain; and an extended domain (colored in blue) were designed to be 18bp that was long enough to stabilize the duplex such that any variation in performance should be caused by the change of destabilization motif.

From PAGE results (Fig. S9, see details of reaction procedure in the main text and Fig. 2A caption), all these motifs were found to perform target recycling successfully and cause negligible leakage except large loop insertion (Set 7).

Recycling performance was shown by comparing the band intensities of lane 2 and 4 respective to their controls (lane 1 and 2), where for all sets other than set 7, negligible I3 and BP were formed (or SP depletion) in absence of recycling; but significant P and BP formation (or SP consumption) was seen when recycling was involved; and under 2.5hr reaction time, saturation almost reached as compared with overnight incubation (lane 9).

System leakage, on the other hand, was deduced by comparing the band intensities of lane 1 and 3, which refers to the effect of adding A2 to the reactant mixture of S1 and A1. Other than set 7, similar band intensities of S1 and B1 were seen on both lanes and with little or no product formation on lane 3. This indicates negligible leakage among the system components. However, set 7 where 6nt insertions were introduced to S1, results in significant leakage as seen from the dim band of SP while dark bands of P and BP on lane 3. We believe that the leakage was caused by the adherence of A2 on the F strand of SP (lane 4) due to 1) high local thermal instability of SP; and more importantly 2) the big loop size in which A2 have enough space to drill through and twist to form a helix. The latter could be proved by dramatic leakage reduction after decreasing the loop size by 2nt (set 8).

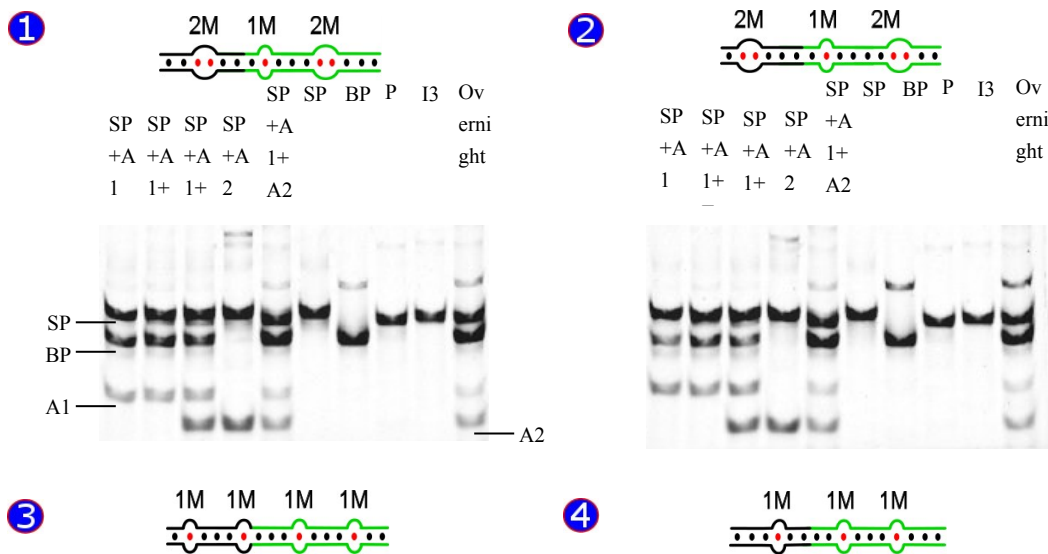




Fig. S9 PAGE gel results to investigate the system leakage and target recycling performance of eight sets of destabilization motifs. Lane 1 and 2: shows performance with and without target under no recycling process; Lane 3 and 4: shows performance with and without target under recycling process; Lane 5-8: markers for S1, B1, P and I2 correspondingly. Lane 9: shows products in the presence of target and recycling process after overnight incubation. For lane 1-4, S1 (F: Q= 1: 1.2) was first reacted with A1 for 20mins to remove excess Q strands; the whole sample was then incubated for 2.5hrs before gel run; [SP] = 400nM, [A1] = 600nM, [A2] = 800nM, [T] = 200nM.

The gel data were further processed to calculate the leakage percentage and fold increase of each set after target recycling. This was achieved by measuring the band intensities of BP using ImageJ (TABLE S1). Note that band intensities of BP were selected for comparison because it was well resolved from other bands. From these data, leakage percentage and fold increase by recycling process were calculated (TABLE S2):

$$Leakage (\%) = \frac{I_{lane 3} - I_{lane 1}}{I_{lane 1}} \times 100\% \quad (21)$$

$$\text{Fold increase by recycling} = \frac{I_{\text{lane 5}} - I_{\text{lane 3}}}{I_{\text{lane 2}} - I_{\text{lane 1}}} \quad (22)$$

In line with above deduction, all motifs show acceptable leakage (from ~0 to < 20%) other than set 7 (80.9%). Among these, destabilization motifs formed by intermittent mismatches result in lower leakage than those of insertions (i.e. lower leakage % of set 1-4 than set 5-6). We observe that through recycling process, signal was increased by more than 2 fold except set 7 where leakage already outperformed that of target analyte.

Please note that this is just a rough estimation over the performance of destabilization motifs using band intensities because of: 1) subjective intensity measurement based on ImageJ; 2) varying loading volume due to capillary action and pipetting error; and 3) indistinguishable band intensities when concentrations of BP become too low or high. This results in underestimated leakage or overestimated recycling performance in short period of time compared to that of overnight incubation, which accounts for the negative values given in set 4 and 7 respectively (TABLE S2, set 4 and 7) as well as the lower values of lane 9 than lane 5 (TABLE S1, set 1-4).

	<i>SI+AI</i> (lane 1)	<i>SI+AI+T</i> (lane 2)	<i>SI+AI+A2</i> (lane 3)	<i>SI+AI+A2+T</i> (lane 5)	<i>Overnight</i> (lane 9)
<i>Set 1</i>	9367.8	10525.3	10057.6	13090.3	12387.1
<i>Set 2</i>	6005.3	8469.8	7089.1	12094.8	11889.3
<i>Set 3</i>	7120.8	8307.2	7300.2	12218.3	11697.5
<i>Set 4</i>	7634.4	8356.9	7563.8	12379.1	11730.7
<i>Set 5</i>	5293.5	6359.8	7518.5	12070.9	12210.0
<i>Set 6</i>	3834.0	5701.1	5752.1	11956.2	12134.1
<i>Set 7</i>	2425.7	4582.7	11471.2	10964.3	11175.7
<i>Set 8</i>	2199.7	4160.4	2941.7	12546.8	12589.0

TABLE S1. Band intensities of BP from the gel image of set 1-8 destabilization motifs measured by ImageJ.

<i>Set</i>	<i>1</i>	<i>2</i>	<i>3</i>	<i>4</i>	<i>5</i>	<i>6</i>	<i>7</i>	<i>8</i>
<i>Leakage (%)</i>	5.6	9.1	1.5	-0.6	18.2	15.8	80.9	5.9
<i>Fold increase by recycling</i>	2.6	2.0	4.1	6.7	4.3	3.3	-0.2	4.9

TABLE S2. Calculated Leakage percentage and fold increase by recycling process of the eight sets of destabilization motifs based on the given intensities of TABLE S1. Other than set 7, the rest shows acceptable leakage and increased signal output through recycling.

S4.2 Effect of the Length of Stabilizing Domain. Long enough sequence base pairing is required to stabilize SP especially when the destabilization motif is introduced. Experiments were then performed to test if varying the length of unrelated domain (blue region) would bring any influence to the system leakage or recycling performance (Fig. S10).

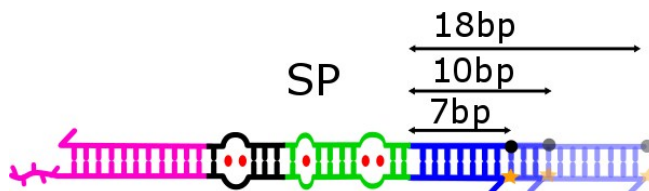
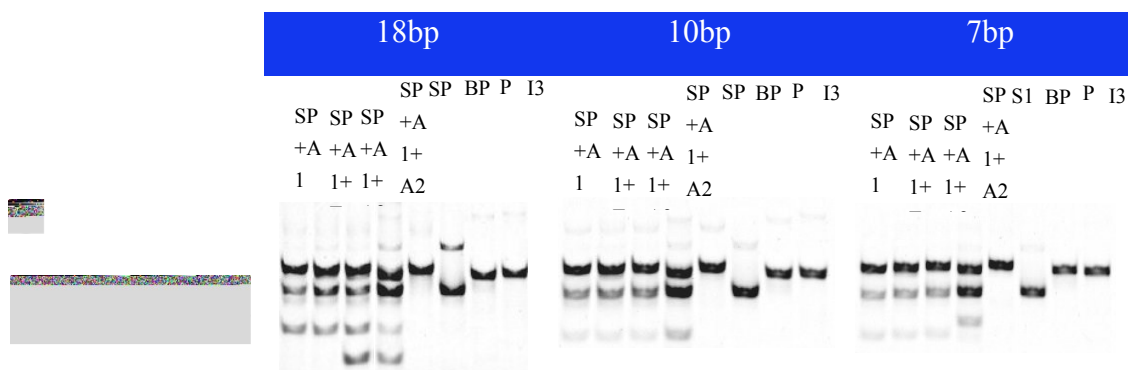


Fig. S10 Test for the effect of shortening length of stabilizing domain of SP (blue region) to the leakage and recycling performance based on set 2 and set 6 destabilization motifs. Shown here corresponds to set 2 motif.

Gel results show that for both set 2 and 6 destabilization motifs, while shortening the length of blue domain either to 10bp or 7bp, leakage remains negligible (see Fig. S11, band intensities of SP, BP and P of lane 3 and 4) and significant product formation was only achieved in the presence of target and recycling process (compare bands of lane 2 and 4 respective to their controls, lane 1 and 3).

Based on the tests on destabilization motifs and unrelated domain length, we selected set 3, having 4 intermittent mismatches as the destabilization motif for specificity measurement in the main Text, while the length of stabilizing domain remains to be 18bp.



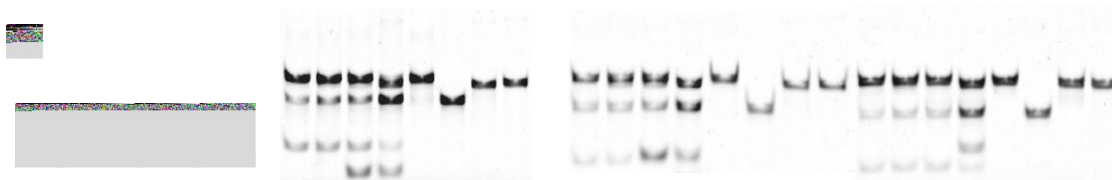


Fig. S11 Gel results testing the effect of the length of stabilization domain (blue domain) of SP to target recycling performance and leakage on set 2 and 6 destabilization motifs. All lanes in the six gels are equivalent. Lane 1 and 2: showing performance in absence and presence of target without recycling process; Lane 3 and 4: showing performance in absence or presence of target with recycling; Lane 5-8: Markers for SP, BP, P and I3 respectively. Component concentrations and reaction conditions are the same as captioned in Fig. S9.

S5. Non-recycling circuit

S5.1 Kinetic result and simulation of non-recycling circuit

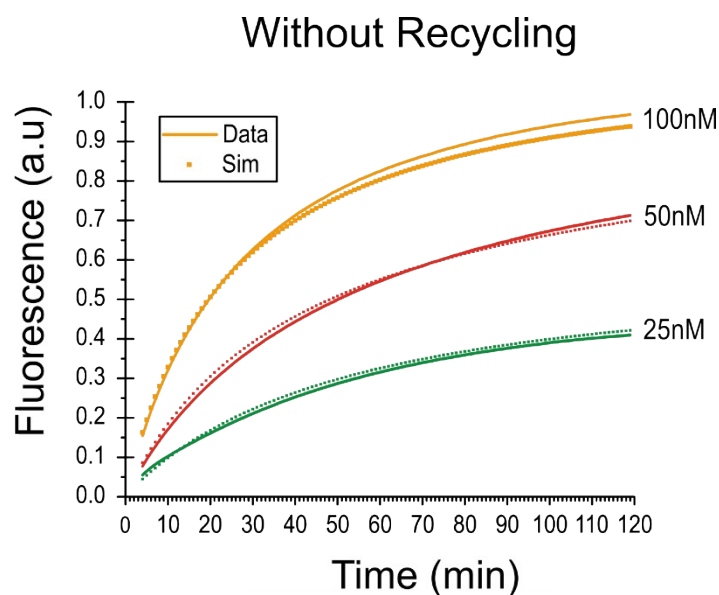


Fig. S12. Kinetic trace without target recycling. Fluorescence data (solid line) were recorded over 2hrs, at $[SP] = 50 \text{ nM}$, $[A1] = 85 \text{ nM}$, $[A2] = 150 \text{ nM}$; and were normalized such that 0 represents the average fluorescence calculated from the negative control (SP + A1); and 1 represents the maximal fluorescence when all SP were consumed (i.e. the fluorescence of 200 nM at 2 hrs). Data before 5 mins were not plotted because fluorescence was not stabilized due to cuvette removal from the cell holder. The dotted lines show simulated results based on the fitted rates constants of the reaction model (Supplementary S7) using fluorescence data of T = 200 nM, 100 nM and 50 nM with recycling.

S5.2 Amplification Efficiency of TRBA

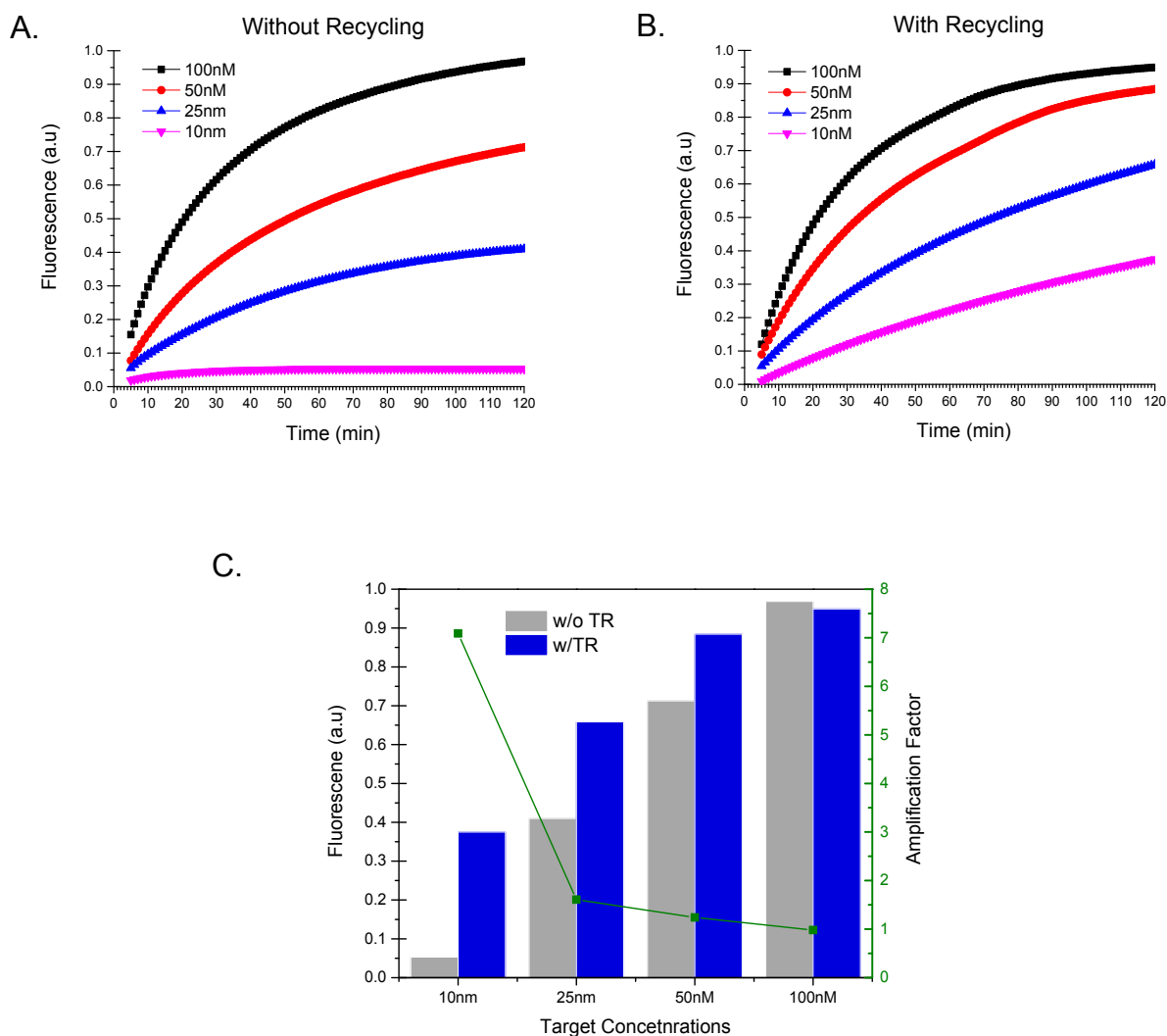


Fig. S13. Kinetic trace A) without and with B) target recycling at target concentrations of 10nM, 25nM, 50nM and 100nM over 2hrs, while [SP]=50 nM, [A1]=85 nM, [A2]=150 nM in both cases. Fluorescence data was normalized such that 0 represents the average fluorescence calculated from the negative control (SP + A1); and 1 represents the maximal fluorescence when all SP were consumed (i.e. the fluorescence of 200 nM at 2 hrs). Data before 5 mins were not plotted because fluorescence was not stabilized due to cuvette removal from the cell holder. C) The column bar chart shows the fluorescence values of the four target concentrations with or without target recycling at the 2hr time-point as obtained from A and B. The amplification factor, or the ratio of their fluorescence values at each concentration was also plotted in green.

S6. Real-time Fluorescence Measurement and Data Processing

S6.1 Data Acquisition. Sensing Probe and other components preparation, as well as settings of the spectrofluorimeter followed the procedures described in the Method section. In all kinetic measurements, solutions were added in two consecutive steps. To ensure thermal equilibrium and stabilization of

fluorescence signal, a solution containing only SP and A1 in 1XTE, 1XPBS buffer (1500 μ l or 1000 μ l for specificity test against target frequencies) was first incubated in the cuvette for 40 mins-1.5 hrs. After reaching stabilization and when the last fluorescence data point soon recorded and appeared in the panel, the cuvette was quickly taken out from the fluorescence cell holder and components required in each run were then added, where the additional volume was all kept at 40 μ l. The cuvette was then capped, vortexed for around 30s and put back to the cell holder to continue the measurement. Although solution may spill onto the inner walls and caps of cuvette during vortexing, we assume this contributes the same, if not little influence to the measurement accuracy for each sample run. This is because the solution volume used in each experimental set was the same, and relatively much higher (1040 μ l or 1540 μ l) than the minimum volume required for the cuvette to give an accurate detection (100 μ l). TABLE S3 shows examples for each experimental set their component concentrations and volume addition.

Sensitivity Measurement (with Recycling), Fig. 2B					
	Solution Concentration		Volume added in first step	Volume added in second step	Final Concentration
Positive Control	SP (2 μ M) and A1 (4 μ M)	and	38.5 μ l		50nM SP, 85nM A1, 15nM BP
	A2 (10 μ M)			23.1 μ l	150nM
	1X TE, PBS		1462 μ l	16.9 μ l	
100nM	SP (2 μ M) and A1 (4 μ M)	and	38.5 μ l		50nM SP, 85nM A1, 15nM BP
	A2 (10 μ M)			23.1 μ l	150nM
	T (20 μ M)			7.7 μ l	100nM
	1X TE, PBS		1462 μ l	9.2 μ l	
500pM	SP (2 μ M) and A1 (4 μ M)	and	38.5 μ l		50nM SP, 85nM A1, 15nM BP
	A2 (10 μ M)			23.1 μ l	150nM
	T (200nM)			3.85 μ l	500pM
	1X TE, PBS		1462 μ l	13.05 μ l	
Sensitivity Measurement (without Recycling), Fig. S12					

100nM	SP (2μM) and A1 (4μM)	38.5μl		50nM SP, 85nM A1 15nM BP
	T (20μM)		7.7μl	100nM
	1X TE, PBS	1462μl	32.3μl	

Specificity Measurement against SBMs (same concentrations as T), Fig. 4A, B

5iC/ /12AtC	SP (2μM) and A1 (4μM)	38.5μl		50nM SP, 85nM A1 15nM BP
	A2 (10μM)		23.1μl	150nM
	SBMs (20μM)		7.7μl	100nM
	1X TE, PBS	1462μl	9.2μl	

Specificity Measurement in mixture of T and SBMs, Fig. 5B, C, E

Positive Control	SP (2μM) and A1 (4μM)	26μl		50nM SP, 85nM A1 15nM BP
	A2 (20μM)		7.8μl	150nM
	1X TE, PBS	974μl	32.2μl	
0%	SP (2μM) and A1 (4μM)	26μl		50nM SP, 85nM A1 15nM BP
	A2 (20μM)		7.8μl	150nM
	SBM mix* (50μM)		20.8μl	1μM
	1X TE, PBS	974μl	11.4μl	
0.5%	SP (2μM) and A1 (4μM)	26μl		50nM SP, 85nM A1 15nM BP
	A2 (20μM)		7.8μl	150nM
	SBM mix* (50μM)	974μl	20.7μl	0.995μM
	T (1μM)		5.2μl	5nM
	1X TE, PBS	1462μl	6.3μl	
5%	SP (2μM) and A1 (4μM)	26μl		50nM SP, 85nM A1 15nM BP
	A2 (20μM)		7.8μl	150nM
	SBM mix* (50μM)	974μl	20.7μl	0.95μM

(50 μ M)			
T (10 μ M)		5.2 μ l	50nM
1X TE, PBS	1462 μ l	6.3 μ l	

* SBM mix was formed by mixing 6mTtC, 9dC, 12AtC and 20TtA.

TABLE S3: Concentrations and volume addition in each experimental set in time-based fluorescence measurements (only selected examples for illustration)

S6.2 Data Processing. The data acquired from fluorescence measurement was modified (FIG. S5) by shifting the time scale such that the time-point where the cuvette was taken out of the cell holder was set to be 0 min, while time before that was in negative values (i.e. the time for thermal equilibrium and fluorescence stabilization). Also, because fluorescence background may differ due to changing cuvette position, lamp intensity fluctuation and pipetting error, we also modified each fluorescence curve by translating it upward and downward, such that their initial fluorescence tracing given by the solution containing only SP and A1 was aligned with that of negative control (SP and A1). In sensitivity measurements (Fig. 1B and S12), the fluorescence values were normalized where 0 refers to the average fluorescence signals calculated from the negative control, while 1 represents the maximum fluorescence value achieved when all SP were reacted (i.e. the end-point in 200nM fluorescence curve). In other measurements, the average fluorescence of negative control from time= 5min to the end of measurement was set at 0, while fluorescence values were all divided by 1000 forming the arbitrary scale shown in the main text.

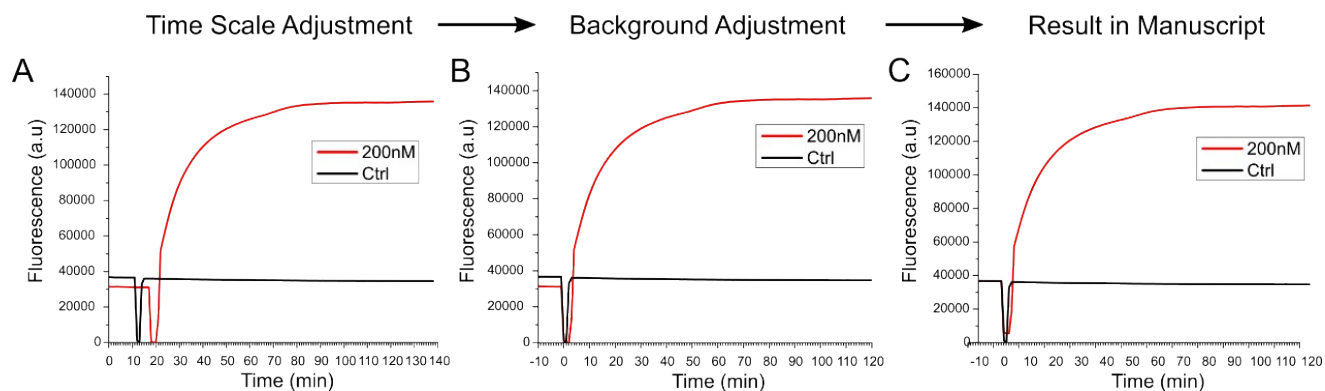
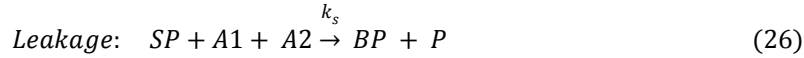
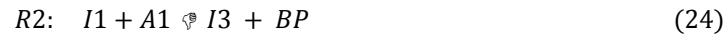


Fig. S14 Processing of fluorescence data by A) shifting the time scale such that the time-point where cuvette was removed from the cell holder for sample addition was set at 0 min; B) translating the fluorescence curve upward or downward such that fluorescence values before t= 0 min aligned on the same level. C) fluorescence curves shown in manuscript after data adjustment by A) and B).

S7. Kinetic Modelling of the Target Recycling Circuit

The reaction mechanism in interacting with long A1 was modelled by breaking down the whole process into three elementary reactions and one for describing system leakage:



where forward and reverse rates of R1, R2 and R3 are $k_1, k_{1r}; k_2, k_{2r};$ and k_3, k_{3r} respectively.

Other branch migration states which formed and consumed rapidly were not included in this modelling. Kinetic simulation of these reactions was then conducted using ode23s function in matlab, where the rate constants for R1, R2 and R3 were fitted by minimizing the square error between the simulated results and real fluorescence data in the sensitivity measurement (200nM, 100nM and 50nM in Fig. 2B). Corresponding matlab codes were shown below:

S7.1 Kinetic simulation

```
function [Output]=recycling(t,input)
T=input(1);
SP=input(2);
I1=input(3);
A1=input(4);
I3=input(5);
BP=input(6);
A2=input(7);
P=input(8);
k1=input(9);
k1r=input(10);
k2=input(11);
k2r=input(12);
k3=input(13);
```

```

k3r=input(14);
ks=input(15);
dT=-k1*SP*T+k1r*I1+k3*I3*A2-k3r*T*P;
dSP=-k1*SP*T+k1r*I1-ks*SP*A1*A2;
dTFQ=k1*SP*T-k2*I1*A1+k2r*I3*BP-k1r*I1;
dA1=-k2*I1*A1+k2r*I3*BP-ks*SP*A1*A2;
dTF=k2*I1*A1-k2r*I3*BP-k3*I3*A2+k3r*P*T;
dQA1=k2*I1*A1-k2r*I3*BP+ks*SP*A1*A2;
dA2=-k3*I3*A2+k3r*P*T-ks*SP*A1*A2;
dA2F=k3*I3*A2-k3r*P*T+ks*SP*A1*A2;
dk1=0;
dk1r=0;
dk2=0;
dk2r=0;
dk3=0;
dk3r=0;
dks=0;
Output=[dT,dFQ,dTFQ,dA1,dTF,dQA1,dA2,dA2F,dk1,dk1r,dk2,dk2r,dk3,dk3r,dks]';

```

S7.2 Error Calculation

```

function Errval=RErr(input)
k1=input(1);
k1r=input(2);
k2=input(3);
data=load('sensitivity data.txt');
SP=50E-9;
Target=[200E-9,100E-9,50E-9];
A1=85E-9;
A2=150E-9;
BP=15E-9;
I1=0;

```

```

I3=0;
P=0;
t0=60;
k2r=0.0593;
k3=6E6;
k3r=4.473E4;
ks=5.38E7;
time=data(:,1)*60-t0;
timebefore=time(time<0);
timeafter=[0;time(time>0)];
time=[timebefore;timeafter];
time=time+t0;
options = odeset('RelTol',1e-4,'AbsTol',1e-20);
Errval=zeros;
for i=1:3
    [t,concentrations] =
ode23s(@notr,timeafter,[Target(i),SP,I1,A1,I3,BP,A2,P,k1,k1r,k2,k2r,k3,k3r,ks],opti
ons);
    conversion=(concentrations(:,8)+concentrations(:,5)+concentrations(:,3))/50E-9;
    conversion=[(0*ones(size(timebefore)))+conversion];
    for j=2:length(conversion)
        if(conversion(j)>=0)
            Errval=Errval+(conversion(j)-data(j-1,15-i))^2;
% data of 200nM, 100nM and 50nM was at the 14th, 13th and 12th column of the data file
        end
    end
end
end
Errval=sum(Errval);

```

S7.3 Rate Constants Fitting

```
clear all;clc;
```

```

minerr = inf;
k1_best = 0;
k1r_best = 0;
k2_best = 0;
for k1= linspace(2,4,30).*10^4
    for k1r=linspace(1,3,30).*10^-1
        for k2=linspace(7,9,30).*10^5
            curr_err=RErr([k1 k1r k2]);
            if (curr_err < minerr)
                minerr=curr_err;
                k1_best = k1;
                k1r_best = k1r;
                k2_best = k2;
            end
            fprintf(' ');
        end
        fprintf('/ ');
    end
    fprintf('!\n');
end
[k1_best k1r_best k2_best]
RErr([k1_best k1r_best k2_best])

```

Note that in our simulation, k_s was fitted by using the fluorescence data from negative control; and best rate constants for k_{2r} , k_3 or k_{3r} were not fitted because we observed that the simulation results were insensitive to the change of these rate constants. Here, we adopted kinetic parameters reported before for simulation,¹ but further kinetic experiments like decoupling the reactions and using an additional reporter instead of incorporating them into the F and Q strands are necessary to confirm the absolute values of these rate constants, although the kinetics estimated will be overestimated due to the loss of fluorophore-quencher pair for stabilization.

S8. Calculation of Discrimination Factor for gel result

The discrimination factor of Fig. 3 C was calculated similar to Text S4 based on the band intensities of

BP using the following equation:

$$Discrimination\ factor = \frac{I_{SBM} - I_{Ctrl}}{I_T - I_{Ctrl}} \quad (27)$$

where I_{SNP} , I_T and I_{Ctrl} represent the band intensities of BP of the single base mutant, target and positive control (SP+A1+A2) respectively measured using ImageJ.

S9. Specificity across Target Positions

S9.1 Quantification of BP for full-length and shortened assistants with Single-base Mutants across Target positions

Intensities of BP in Fig. 4D of the main manuscript were quantified as described in S2. Values in bold indicated the mutants that differed with that of correct target by at least 2000 that these mutants were considered to be differentiable significantly with that of target.

	-ve Ctrl	2dA	3iG	5iA	5iC	6TtC	8TtG	9dC
Full-length A1	5888.1	9277.3	8908.0	8217.9	8454.2	6904.0	8946.6	5994.4
Shortened A1	3142.2	6784.4	4654.0	3281.4	3399.4	3664.9	4284.9	3062.6

	10iT	12AtC	13CtG	17TtG	20TtC	21GtC	22AtC	T
Full-length A1	9657.4	7952.5	9725.2	8945.2	5763.7	9179.1	9381.4	9084.2
Shortened A1	3236.9	3748.0	4630.2	5097.3	3494.4	5093.6	6013.4	9259.3

Table S4. The band intensities of the 14 mutants using full-length or shortened A1

S9.2 $\Delta \Delta G$ Calculation of 14 Single-base Mutants

The $\Delta\Delta G$ shown in Fig. 4E was calculated by the difference of reaction Gibbs free energies between T and SBM, where

$$\Delta\Delta G = \Delta G_{SBM} - \Delta G_T \quad (28)$$

Because specificity was contributed mainly by the rate-limiting target hybridization step, while less likely by the analyte displacement step due to spontaneity and excess amounts of A2 used in the reaction, their Gibbs free energy difference can be simplified by solely considering the overall equations derived from R1 and R2:



Based on these equations, reaction Gibbs free energies can then be calculated by subtracting the Gibbs free energies of products by their reactants, for example:

$$\Delta G_T = G_{BP} + G_{I3_T} - G_{SP} - G_{A1} - G_T \quad (29)$$

$$\Delta G_{SBM} = G_{BP} + G_{I3_{SBM}} - G_{SP} - G_{A1} - G_{SBM} \quad (30)$$

And therefore,

$$\Delta\Delta G = G_{I3_{SBM}} - G_{SBM} - G_{I3_T} + G_T \quad (31)$$

where Gibbs free energies of these components were calculated using Nupack, by setting temperature= 25°C, Na⁺ concentration= 0.154M, dangle=some/all. The corresponding values and $\Delta\Delta G$ which was calculated by taking the average values from some and all dangles of all 14 SBMs were shown in TABLE S5.

SBM\Dangle	$G_{I3_{SBM}}$ (kcal/mol)			G_{SBM} (kcal/mol)			$\Delta\Delta G$ (kcal/mol)*		
	Some	All	Average	Some	All	Average	Some	All	Average
2dA	-28.9	-28.94	-28.92	-2.11	-2.13	-2.12	1.33	1.66	1.495
3iG	-28.85	-28.91	-28.88	-2.31	-2.34	-2.325	1.58	1.9	1.74
5iA	-26.82	-24.81	-25.815	-2.4	-2.42	-2.41	3.7	6.08	4.89
5iC	-27.12	-27.51	-27.315	-2.13	-2.17	-2.15	3.13	3.13	3.13
6TtC	-26.1	-26.46	-26.28	-3.52	-3.52	-3.52	5.54	5.53	5.535
8TtG	-28.04	-28.41	-28.225	-1.67	-1.71	-1.69	1.75	1.77	1.76
9dC	-24.65	-25.01	-24.83	-0.99	-1.09	-1.04	4.46	4.55	4.505
10iT	-26.61	-26.98	-26.795	-1.53	-1.61	-1.57	3.04	3.1	3.07
12AtC	-25.5	-25.86	-25.68	-2.36	-2.4	-2.38	4.98	5.01	4.995
13CtG	-27.72	-28.09	-27.905	-2.09	-2.11	-2.1	2.49	2.49	2.49
17TtG	-27.62	-27.99	-27.805	-1.54	-1.6	-1.57	2.04	2.08	2.06
20TtC	-26.53	-26.89	-26.71	-2.3	-2.34	-2.32	3.89	3.92	3.905
21GtC	-27.28	-27.65	-27.465	-2.14	-2.17	-2.155	2.98	2.99	2.985
22AtC	-29.32	-29.68	-29.5	-2.23	-2.25	-2.24	1.03	1.04	1.035

* $\Delta\Delta G$ of all SBMs were calculated by adding G_T : -2.13 kcal/mol (some), -2.14 kcal/mol (all), -2.14 kcal/mole (average); and subtracting G_{I3_T} : -30.25 kcal/mol (some), -30.62 kcal/mol (all), -30.435 kcal/mol (average).

Table S5. The Gibbs free energies of 14 SBMs, corresponding I3 and the $\Delta\Delta G$ calculated based on Nupack Software

S10. Oligonucleotides Sequence Design

Sequences of SP, A1 and A2 were designed using Nupack such that:

- 1) There was negligible interaction or crosstalk among components
- 2) The destabilization motif was stably formed within SP
- 3) Assistants were designed with negligible secondary structures
- 4) Sequence was designed based on the chosen target analyte, microRNA 21

To reduce leakage due to fraying of strands at mismatch or insertion bubbles, as well as the duplex ends, 2nt clamping were inserted at the blunt ends of SP, while A1 and A2 were designed with 2nt truncated at 3' ends such that they were unable to attack SP even when the last two base pairs of its duplex ends were dissociated. Also, strong G-C pair was adopted in region with high chances of fraying or breathing, for example, at the end of duplex and contiguous base pairs of the mismatch or insertion bubbles, to further lower leakage. Table S6 shows all sequences used in this manuscript.

A. Destabilization Motif Characterization		
Set 1-6	F strand	TCAAC AT CAGTCTGAT AAGCTA ATACACGCAA TAGAAGTAGATCCAAG GC
	A2	GCGTGTAT TAGCTT ATCAGACTG
Set 7-8	F strand	TCAAC AT CAGTCTGAT AAGCTA TAACGTGTAA AGAATGTAGATCCAAG GC
	A2	TTACACGTTA TAGCTT ATCAGACTG
Set 1	Q strand	GC CTTGGATCTACTTCTA TTGGTTGTCT TACGTT ATCAGACTG AT
	A1	AACGTA AGACAACCAA TAGAAGTAGATCCAAG
Set 2	Q strand	GC CTTGGATCTACTTCTA TTCAGTGTCT TAGGAT ATCAGACTG AT
	A1	ATCCTA AGACACTGAA TAGAAGTAGATCCAAG
Set 3	Q strand	GC CTTGGATCTACTTCTA TTTCGTTTAT GAGCGT ATCAGACTG AT
	A1	ACGCTC ATAACGAAA TAGAAGTAGATCCAAG
Set 4	Q strand	GC CTTGGATCTACTTCTA TTGGGTGGAT TA A CTT ATCAGACTG AT
	A1	AAGTTA ATCCACCAA TAGAAGTAGATCCAAG

Set 5	Q strand	GC CTTGGATCTACTTCTA TTG_GTG_AT TA_CTT ATCAGACTG AT
	A1	T AAG_TA AT_CAC_CAA TAGAAGTAGATCCAAG
Set 6	Q strand	GC CTTGGATCTACTTCTA TTG_GTG_AT TA__TT ATCAGACTG AT
	A1	AT AA_TA AT_CAC_CAA TAGAAGTAGATCCAAG
Set 7	Q strand	GC CTTGGATCTACATTCT TTAC_____ TAGCTT ATCAGACTG AT
	A1	AAGCTA_____GTAA AGAATGTAGATCCAAG
Set 8	Q strand	GC CTTGGATCTACATTCT TTACAC_____ TAGCTT ATCAGACTG AT
	A1	AAGCTA_____GTGTAA AGAATGTAGATCCAAG

B. Effect of the length of stabilization domain			
Set 2	7 bases	Q strand	CC TTCTA TTCAGTGTCT TAGGAT ATCAGACTG AT
		F strand	TCAAC AT CAGTCTGAT AAGCTA ATACACGCAA TAGAA GG
		A1	ATCCTA AGACACTGAA TAGAA
	10 bases	Q strand	GT TACTTCTA TTCAGTGTCT TAGGAT ATCAGACTG AT
		F strand	TCAAC AT CAGTCTGAT AAGCTA ATACACGCAA TAGAAGTA AC
		A1	ATCCTA AGACACTGAA TAGAAGTA
Set 6	7 bases	Q strand	CC TTCTA TTG_GTG_AT TA_TT ATCAGACTG AT
		F strand	TCAAC AT CAGTCTGAT AAGCTA ATACACGCAA TAGAA GG
		A1	AT AA_TA AT_CAC_CAA TAGAA
	10 bases	Q strand	GT TACTTCTA TTG_GTG_AT TA__TT ATCAGACTG AT
		F strand	TCAAC AT CAGTCTGAT AAGCTA

		AT <u>A</u> CACGCAA TAGAAGTA AC
A1		AT AA_ TA AT_CAC_CAA TAGAAGTA

C. Interaction with Shortened A1 and Necessity of Mismatches		
A1	-2nt	GCTC <u>ATA</u> <u>A</u> CG <u>AA</u> TAGAAGTAGATCCAAG
	-4nt	TC <u>ATA</u> <u>A</u> CG <u>AA</u> TAGAAGTAGATCCAAG
	-6nt [^]	<u>ATA</u> <u>A</u> CG <u>AA</u> TAGAAGTAGATCCAAG
	-7nt	<u>TA</u> <u>A</u> CG <u>AA</u> TAGAAGTAGATCCAAG
	m3*	ATACACG <u>AA</u> TAGAAGTAGATCCAAG
	m4 [#]	ATAC <u>A</u> CGCAA TAGAAGTAGATCCAAG
Q strand	m4	GC CTTGGATCTACTTCTA <u>TT</u> <u>A</u> CGTGTAT TAGCTT ATCAGACTG AT
	m14	GC CTTGGATCTACTTCTA <u>TT</u> <u>A</u> CGTGTAT TAGCGT ATCAGACTG AT
	m24	GC CTTGGATCTACTTCTA <u>TT</u> <u>A</u> CGTGTAT <u>G</u> AGCTT ATCAGACTG AT
	m34	GC CTTGGATCTACTTCTA <u>TT</u> <u>A</u> CGT <u>T</u> TAT TAGCTT ATCAGACTG AT
	m13	GC CTTGGATCTACTTCTA <u>TT</u> GCGT <u>T</u> TAT TAGCGT ATCAGACTG AT
	m23	GC CTTGGATCTACTTCTA <u>TT</u> GCGT <u>T</u> TAT <u>G</u> AGCTT ATCAGACTG AT
	m123	GC CTTGGATCTACTTCTA <u>TT</u> GCGT <u>T</u> TAT <u>G</u> AGCGT ATCAGACTG AT
	m124	GC CTTGGATCTACTTCTA <u>TT</u> <u>A</u> CGTGTAT <u>G</u> AGCGT ATCAGACTG AT

* m3_A1 was used to interact with SP formed by m13, m23 and m123 Q strands; # m4_A1 was used to interact with SP formed by m4, m14, m24 and m124 Q strands; and [^]-6nt_A1 was used to interact with SP formed by m34 and m1234.

D. T , poly T strand and 14 SBMs

T	TAGCTT ATCAGACTG AT GTTGA
Poly T strand	TTTTT TTTTT TTTTT TTTTT
2dA	T <u>G</u> CTT ATCAGACTG AT GTTGA
3iG	TAG <u>G</u> CTT ATCAGACTG AT GTTGA
5iA	TAGC <u>A</u> TT ATCAGACTG AT GTTGA
5iC	TAGC <u>C</u> TT ATCAGACTG AT GTTGA
6TtC	TAGCT <u>T</u> ATCAGACTG AC GTTGA
8TtG	TAGCTT A<u>G</u>CAGACTG AT GTTGA
9dC	TAGCTT AT<u>A</u>GACTG AT GTTGA
10iT	TAGCTT ATC<u>T</u>AGACTG AT GTTGA
12AtC	TAGCTT ATCAG<u>C</u>CTG AT GTTGA
13CtG	TAGCTT ATCAG<u>A</u>GTG AT GTTGA
17TtG	TAGCTT ATCAGACTG <u>A</u>G GTTGA
20TtC	TAGCTT ATCAGACTG AT GT<u>C</u>GA
21GtC	TAGCTT ATCAGACTG AT GTT<u>C</u>A
22AtC	AAGCTT ATCAGACTG AT GTTGA<u>A</u>

TABLE S6: Sequences used in this manuscript

References

- (1). Zhang, D. Y.; Winfree, E. *J. Am. Chem. Soc.* **2009**, *131*, 17303-17314.